2024 Tenth Indian Control Conference (ICC)
9 - 11 December, 2024
IISER Bhopal, India

Classical-Control-Centric Characterization of Conservativeness in Mixed-Sensitivity Synthesis for SISO Systems

Potluri Ramprasad and Thota Vishnudatta

***Abstract*— For a given plant, closed loopshaping (CLS) aims to synthesize a feedback controller under separate constraints on the H-infinity norms of the weighted sensitivity and weighted complementary sensitivity functions. Mixed-sensitivity synthesis (MSS) attempts to perform CLS by constraining the H-infinity norm of the vector formed by stacking these two functions. It is known that MSS is therefore conservative compared to CLS. However, a classical-control-centric graphical characterization of this conservativeness seems to be absent. For single-input single-output plants, this paper provides this characterization, and therefrom presents a nonconservative approach to CLS.**

I. Introduction

For a single-input single-output (SISO) plant with the transfer function (TF) $G(s)$ a basic problem is to design a controller TF $C(s)$, such that the control system of Fig. 1 satisfies certain frequency-domain performance specifications. Before the advent of computers and convenient software, such as Matlab, this problem used to be posed as one of *loopshaping* [1], [2]. Loopshaping involves shaping the loop gain $|L(j\omega)|$ of the loop TF $L(s)=C(s)G(s)$ by hand on semilog paper. See [3] for historical notes on loopshaping.

On the semilog grid loopshaping divides the operating frequencies of the control system into low-frequency (LF), mid-frequency (MF), and high-frequency (HF) areas, and shapes the loop gain in each area to satisfy the specifications for that area. In particular, the loop gain needs to stay above an LF forbidden region specifying tracking performance and disturbance rejection, and needs to stay below an HF forbidden region specifying noise rejection, gain margin, and strict properness of $C(s)$. In the vicinity of the gain crossover frequency ω_g (MF area), the slope and width of the loop gain help meet specified phase margin, peak overshoot, etc, while ω_g helps meet specified settling time. Fig. 2(a) shows a typical loop shape [4, p.322], [5, pp.631–632], [6], [7]. Loopshaping mainly addresses minimum-phase $G(s)$, but with minor modifications applies to non-minimum-phase $G(s)$ [2, pp. 44–46], and unstable $G(s)$ too.

In robust control, the HF forbidden region additionally specifies robustness against norm-bounded multiplicative uncertainties [2, p.276], since a plant model is most inaccurate in the HF region [2, Section 7.4], [8].

Closed loopshaping (CLS) is an alternative to loopshaping. CLS aims to design $C(s)$ such that, for the sensitivity and complementary sensitivity functions

$$S(s)=1/(1+L(s)),\quad T(s)=L(s)/(1+L(s)), \tag{1}$$

R. Potluri (e-mail: potluri@iitk.ac.in) is with the Department of Electrical Engineering, IIT Kanpur, Kanpur, India 208016. V. Thota (tvishnudatta@gmail.com) has a BTech degree (2024) from this department.

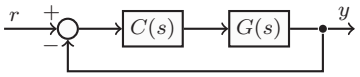


Fig. 1. A unity-feedback closed-loop system.

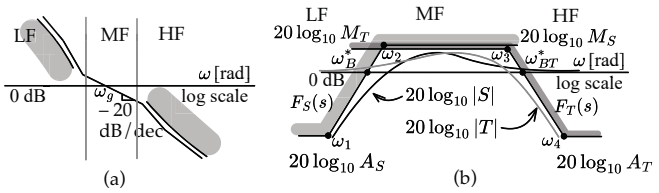


Fig. 2. Loopshaping (a) and closed loopshaping (b).

TFs $F_S(j\omega)\equiv\frac{1}{w_P(j\omega)}$ and $F_T(j\omega)\equiv\frac{1}{w_T(j\omega)}$ upper bound $|S(j\omega)|$ and $|T(j\omega)|$ as in Fig. 2(b) as

$$\left.\begin{aligned}|w_P(j\omega)S(j\omega)|&=\left|\frac{S(j\omega)}{F_S(j\omega)}\right|<1,\\ |w_T(j\omega)T(j\omega)|&=\left|\frac{T(j\omega)}{F_T(j\omega)}\right|<1.\end{aligned}\right\} \tag{2}$$

H_∞ CLS aims to design $C(s)$ for the general case of $G(s)$ being a multi-input multi-output transfer function, such that $\|w_P(s)S(s)\|_\infty<1$ and $\|w_T(s)T(s)\|_\infty<1$. *Mixed-sensitivity synthesis* (MSS) aims to perform H_∞ CLS by designing $C(s)$ such that $\left\|\binom{w_PS}{w_TT}\right\|_\infty<1$. For SISO systems, this inequality reduces to

$$|w_P(j\omega)S(j\omega)|^2+|w_T(j\omega)T(j\omega)|^2<1. \tag{3}$$

See [2, Section 2.8] for an introduction to these topics.

On the 2-D plane with $|w_PS|$ and $|w_TT|$ along the axes, as in Fig. 3(a), (2) describes the first-quadrant part of a square area centered at the origin, while (3) describes the first-quadrant part of a circular disc inscribed in this square area. Thus, MSS does not see some solutions of CLS, and thus is conservative or limited. Nevertheless, MSS is popular, especially for SISO systems [9], [10], [11], and Matlab [12] and GNU Octave implement it as the function *mixsyn*.

For SISO systems, as its first contribution, this paper characterizes the conservativeness of the MSS in two steps: (1) it translates the CLS and MSS problems onto the Nyquist plane and semilog grid, and (2) compares the gain margin (GM), phase margin (PM), and forbidden regions for $L(j\omega)$ and their dimensions in the two problems. This characterization seems to be absent in the literature, though [13] has solved the reverse problem of translating GM and PM specifications into the H_∞ framework. This characterization helps alleviate the problem of absence of insight, among others,

that [14] mentions for both SISO CLS and MSS; [14] too translates closed-loop constraints to the open loop domain. This characterization helps present the second contribution: a nonconservative loopshaping solution to the CLS problem.

The remainder of this paper is as follows. Section II presents two preliminary translations of (2) and (3). Section III presents the first contribution, while Section III-C and the example of Section IV present the second contribution. Section V concludes with directions for future research.

II. From T and S to L: Initial Solution

Section II-A attempts to infer as much as possible about $|L(j\omega)|$ from (2) and (3), without going to the Nyquist plane. Section II-B describes $L(j\omega)$ exactly using (2) and (3).

A. Some Insights from $|w_PS|$ - $|w_TT|$ Plane

Fig. 3(a) shows that the maximum difference between the search spaces of CLS and MSS is along the direction $|w_PS|=|w_TT|$. Specifically, (2) allows $|w_PS|=|w_TT|=1$, while (3) allows $|w_PS|=|w_TT|=\frac{1}{\sqrt{2}}$. This paper explores the implications of this difference for the loop shape.

Fig. 3(a) shows three divisions in the solution sets of (2) and (3). These divisions map to the magnitude-frequency plane. On this plane, the inequality $|L|>|F_T/F_S|$ of the upper division may be an accurate lower bound on $|L|$ and the inequality $|L|<|F_T/F_S|$ of the lower division may be an accurate upper bound on $|L|$. It remains to identify the frequency areas over which these bounds apply. However, since it is already a thumb rule that $|L|$ needs to have high LF gain and low HF gain (see (13) and (14)) as in Fig. 2 (a), this identification is less crucial than examining the MF area.

The maximum difference between the CLS and MSS is in the middle division ($|L|=|F_T/F_S|$). The point $|L|=1$ on this division maps to ω_g. Therefore, this division is related to MF area. Thus, the worst-case conservativeness of (3) relative to (2) may be in this area. Consequently, this paper pays the most attention to the MF area.

Fig. 3(b) shows a sample loop shape arising from the above discussion. The loop shape as well as the constraining curve $|F_T/F_S|$ are smooth, because the forbidden regions in Fig. 2(b) have TF representation, such as [2]

$$F_S(s) = A_S\left(\frac{\frac{s}{\omega_1}+1}{\frac{s}{\omega_2}+1}\right)^{n_1} = A_S\frac{\left(\frac{s}{\omega_B^* {A_S}^{1/n_1}}+1\right)^{n_1}}{\left(\frac{s}{\omega_B^* {M_S}^{1/n_1}}+1\right)^{n_1}}, \quad (4)$$

$$F_T(s) = M_T\left(\frac{\frac{s}{\omega_4}+1}{\frac{s}{\omega_3}+1}\right)^{n_1} = M_T\frac{\left(\frac{{A_T}^{1/n_1}}{\omega_{BT}^*}s+1\right)^{n_1}}{\left(\frac{{M_T}^{1/n_1}}{\omega_{BT}^*}s+1\right)^{n_1}}. \quad (5)$$

B. Exact Characterization

This subsection converts the closed-loop constraints (2) and (3) into constraints on $L(j\omega)$. The essence of this conversion is the same that underlies the classical concept of *M-circles* [4], [15], which is to express $L(j\omega)$ as

$$L(j\omega) = L_x(\omega) + jL_y(\omega). \quad (6)$$

The remainder of this subsection uses (6) in (2) and (3).

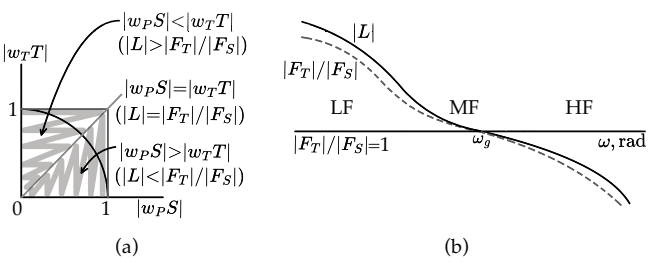


Fig. 3. A quick loopshaping insight from (2) and (3).

1) From Constraining S to Constraining L: Consider the constraint $|S|=|S(j\omega)|<|F_S|=|F_S(j\omega)|$ from (2), with $S(s)$ as in (1). Representation (6) allows writing this constraint as

$$(L_x(\omega)+1)^2+{L_y(\omega)}^2>{R_S}^2 = 1/|F_S|^2 \quad (7)$$

On the Nyquist plane, (7) requires $L(j\omega)$ to be outside a circular disc centered at $(-1,0)$ and of radius $R_S=\frac{1}{|F_S(j\omega)|}$.

2) From Constraining T to Constraining L: Consider the constraint $|T|=|T(j\omega)|<|F_T|=|F_T(j\omega)|$ from (2), with $T(s)$ as in (1). Representation (6) allows writing this constraint as

$$\left.\begin{pmatrix}(L_x(\omega)-C_T(\omega))^2+{L_y(\omega)}^2<R_T^2(\omega),\\ C_T(\omega)=\frac{|F_T|^2}{1-|F_T|^2}, R_T(\omega)=\frac{|F_T|}{1-|F_T|^2}\end{pmatrix},|F_T|<1\right\}$$
$$\left.\begin{pmatrix}(L_x(\omega)-C_T(\omega))^2+{L_y(\omega)}^2>R_T^2(\omega),\\ C_T(\omega)=\frac{|F_T|^2}{1-|F_T|^2}, R_T(\omega)=\frac{|F_T|}{|F_T|^2-1},\end{pmatrix},|F_T|>1\right\} \quad (8)$$

On the Nyquist plane, (8) requires $L(j\omega)$ to be inside (for $|F_T(j\omega)<1|$) or outside (for $|F_T(j\omega)>1|$) a circular disc centered at $(C_T(\omega),0)$ and of radius $R_T(\omega)$.

In summary, the discs in sections II-B.1 and II-B.2, taken together, give the forbidden region for $L(j\omega)$ on the Nyquist plane, and represent the CLS constraints (2).

3) From MSS Constraints on S and T to Constraining L: Representation (6) allows writing constraint (3) as

$$\left.\begin{pmatrix}(L_x(\omega)-C_\mu(\omega))^2+{L_y(\omega)}^2<R_\mu^2(\omega),\\ C_\mu=\frac{|F_T|^2}{1-|F_T|^2}, R_\mu=\frac{|F_T|}{|F_S|}\frac{\sqrt{|F_T|^2+|F_S|^2-1}}{1-|F_T|^2},\end{pmatrix},|F_T|<1\right\}$$
$$\left.\begin{pmatrix}(L_x(\omega)-C_x(\omega))^2+{L_y(\omega)}^2>R_\mu^2(\omega),\\ C_\mu=\frac{|F_T|^2}{1-|F_T|^2}, R_\mu=\frac{|F_T|}{|F_S|}\frac{\sqrt{|F_T|^2+|F_S|^2-1}}{|F_T|^2-1},\end{pmatrix},|F_T|>1\right\} \quad (9)$$

The observations about (8) are relevant here too. Further, the centers are the same, that is, $C_\mu=C_T$; only the radii are different. Note that, in the absence of $F_S(s)$ (equivalently $|F_S(j\omega)|\to\infty$), (9) reduces to (8), and in the absence of $F_T(s)$ (equivalently $|F_T(j\omega)|\to\infty$), (9) reduces to (7).

Constraints (7), (8), and (9) are too unwieldy to sketch by hand. Therefore, they lack one of the main advantages of classical control theory. The remainder of this paper offers a solution that aids quick sketching by hand. This solution focuses only on the constraints from Fig. 2(b) over $\omega \in (0,\omega_B^*)\cup(\omega_2,\omega_3)\cup(\omega_{BT}^*,\infty)$, approximately.

III. On Nyquist Plane and Semilog Grid

Define $m_S \triangleq \max_\omega |S(j\omega)|$ and $m_T \triangleq \max_\omega |T(j\omega)|$. Fig. 2(b) requires $m_S \le M_S$ and $m_T \le M_T$.

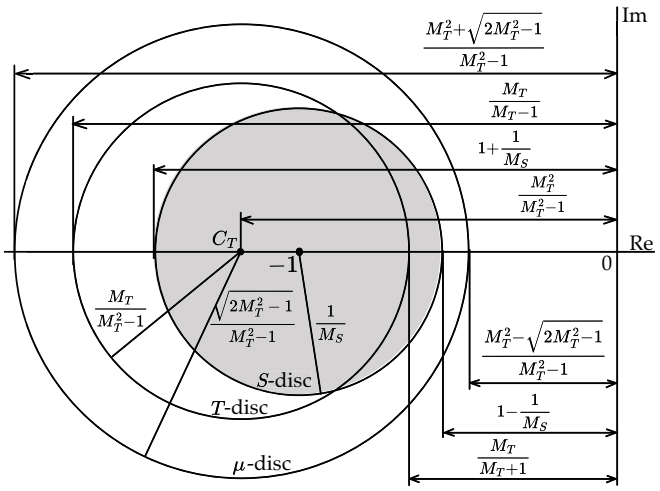


Fig. 4. Comparison of discs for $M_S = M_T > 1$.

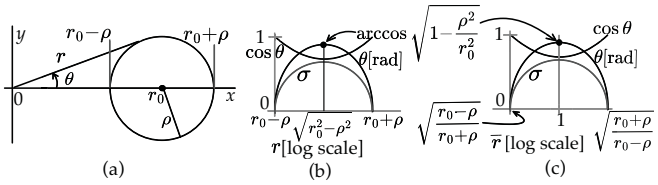


Fig. 5. Construction aiding in the derivation of some properties of circles.

"Typically, it is required that m_S is less than about 2 (6 dB) and m_T is less than about 1.25 (2 dB). A large value of m_S or m_T (larger than about 4) indicates poor performance as well as poor robustness." [2, p.36]. Further, $|m_S - m_T| \leq 1$; see Appendix A. With these considerations, for simplicity, this paper chooses $M_S = M_T$.

A. Some Basics

1) Discs for $M_S = M_T > 1$: Figure 4 shows discs named here *S-disc*, *T-disc*, and *μ-disc*, corresponding, respectively, to (7), (8), and (9), for the case of $F_S = M_S = F_T = M_T > 1$. Here are several notes about these discs.

For $M_T > 1$, the center of S-disc lies within T-disc (since $\frac{M_T}{M_T+1} < 1$), to the right of the center of T-disc, since $C_T < -1$. For $M_T > 1$, $M_S > 1$, S-disc is closer than T-disc to the origin, since $1 - \frac{1}{M_S} < \frac{M_T}{M_T-1}$.

For $M_T = M_S > 1$, the center of T-disc lies within S-disc, since $1 + \frac{1}{M_S} > \frac{M_T^2}{M_T^2-1}$; T-disc is larger than S-disc, since $R_T > R_S$; and μ-disc is closer than S-disc to the origin, since $\frac{{M_T}^2 - \sqrt{2{M_T}^2-1}}{{M_T}^2-1} < 1 - \frac{1}{M_S}$.

Along with the fact that $C_\mu = C_T$, this last inequality implies that μ-disc contains S-disc and T-disc, and is thus larger than the union of S-disc and T-disc when $M_S = M_T > 1$. Section III-B shows that this observation explains in the language of classical control why MSS is conservative in comparison to CLS.

Remark 1: With $M_S, M_T > 1$, how is the choice $M_S \neq M_T$ useful? This question is left for future investigation.

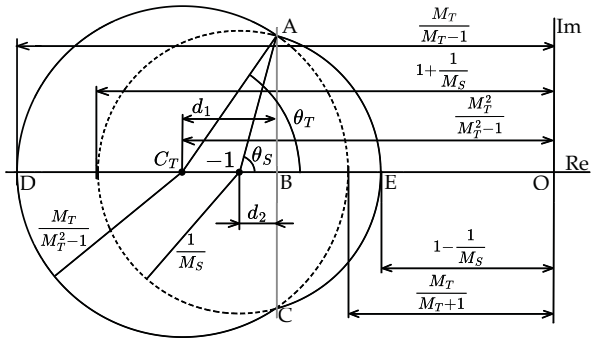


Fig. 6. Union of S-disc and T-disc. The solid outline encloses this union.

m_T	1.1	1.3	1.5	1.7
$M_p\%$	13.8	26.5	37.2	44.6

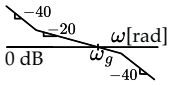


Fig. 7. Correlation between M_p and m_T for a minimum-phase $T(s)$ corresponding to a $\{-40, -20, -40\}$ dB/dec loopgain for $F_S(s)$ not specified, that is, $M_S > M_T + 1$. [7, p.378].

2) Circle in Polar Coordinates: The equation of a circle centered at (r_0, θ_0) and of radius ρ in the polar coordinates (r, θ) is $r^2 + r_0^2 - 2rr_0\cos(\theta - \theta_0) = \rho^2$. For $\theta_0 = 0$, as shown in Fig. 5(a), this equation is $r^2 + r_0^2 - 2rr_0\cos\theta = \rho^2$, giving

$$\cos\theta = \left(r^2 + (r_0^2 - \rho^2)\right)/(2rr_0). \tag{10}$$

Using $\overline{r} := \frac{r}{\sqrt{r_0^2-\rho^2}}$, (10) is $\cos\theta = Y(\overline{r}) := \frac{\overline{r}^2+1}{\overline{r}} \frac{\sqrt{r_0^2-\rho^2}}{2r_0}$.

For $r_0 > \rho$, figures 5(b) and 5(c) show the plots of $\cos\theta$ vs. r and $\cos\theta$ vs. $\overline{r}$, respectively, as the pair (r, θ) traces the upper semicircle in Fig. 5(a). These plots have the minima

$$\cos\theta = \sqrt{1 - (\rho^2/r_0^2)}. \tag{11}$$

Since $Y(\overline{r}_1^\varepsilon) = Y(\overline{r}_2^\varepsilon)$, $\overline{r}_1 = \frac{1}{\overline{r}_2} = \sqrt{\frac{r_0-\rho}{r_0+\rho}}$, $0 < \varepsilon < 1$, it follows that $\cos\theta$ vs. $\log_{10} r$ is symmetric about the vertical line through $r = \sqrt{r_0^2 - \rho^2}$. Finally, it can be verified that a point with a given abscissa on θ vs. $\overline{r}$ curve is above the point with the same abscissa on the semicircle σ. That is, the θ vs. r curve is not circular.

Remark 2: It would be interesting to have a closed-form expression for $\theta = \arccos\frac{r^2 + (r_0^2 - \rho^2)}{2rr_0}$ vs. $\log_{10} r$.

3) Correlation between m_T and Peak Overshoot: There exists a correlation between the peak overshoot $M_p\%$ of the unit step response of $T(s)$ and the peak m_T of $|T(j\omega)|$. For example, Fig. III-B shows this correlation for a minimum-phase $L(s)$ whose asymptotic Bode magnitude plot (ABMP) has the form $\{-40, -20, -40\}$ dB/dec around the gain crossover frequency ω_g. For $T(s) = \frac{\omega_n}{s^2 + 2\zeta s + \omega_n^2}$, $0 < \zeta < 1$, [2, p.38] too has such a table for $1 \leq m_T \leq 50$ and $1 \leq m_S \leq 50$.

B. Characterization on Nyquist Plane

Fig. 6 shows the union of S-disc and T-disc, named here *ST-union*, outlined by the solid line. One way to characterize the conservativeness introduced by mixed sensitivity is through PM and GM. The other way is by comparing the area A_μ of μ-disc with the area $A_\cup$ of ST-union.

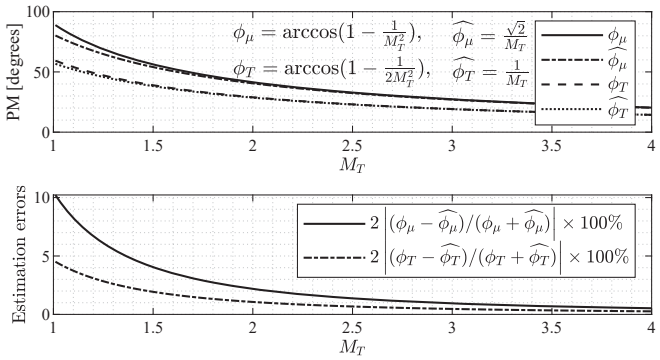


Fig. 8. Estimates of ϕ_μ and ϕ_T.

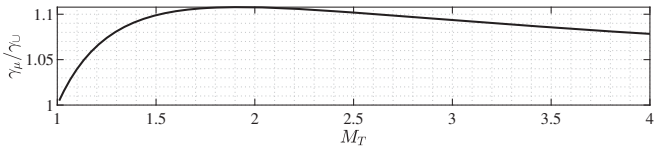


Fig. 9. Ratios of GMs required by μ-disc and the ST-union.

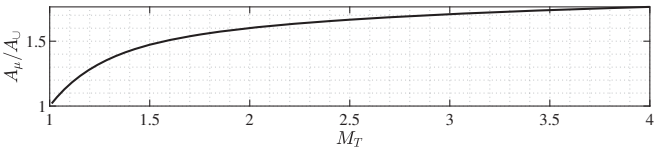


Fig. 10. $A_\mu/A_\cup$ vs. M_T.

1) PM way: By definition, PM is measured at $|L(j\omega)|=1$. Let ϕ_S, ϕ_T, and ϕ_μ respectively be the PMs that S-disc, T-disc, and μ-disc require. For S-disc, substituting $r=|L(j\omega)|=1$, $r_0=1$, and $\rho=\frac{1}{M_S}$ into (10) gives $\cos\phi_S=1-\frac{1}{2M_S^2}$. For T-disc, substituting $r=|L(j\omega)|=1$, $r_0=|C_T|=\frac{M_T^2}{M_T^2-1}$, and $\rho=R_T=\frac{M_T}{M_T^2-1}$ into (10) gives $\cos\phi_T=1-\frac{1}{2M_T^2}$. For μ-disc, substituting $r=|L(j\omega)|=1$, $r_0=|C_T|=\frac{M_T^2}{M_T^2-1}$, and $\rho=R_\mu=\frac{\sqrt{2M_T^2-1}}{M_T^2-1}$ into (10) gives $\cos\phi_\mu=1-\frac{1}{M_T^2}$.

Using the first-order approximation $\cos\theta\approx 1-\frac{\theta^2}{2!}$ of the series expansion $\cos\theta=1-\frac{\theta^2}{2!}+\frac{\theta^4}{4!}-\dots$ with the results in the previous paragraph gives the estimates

$$\widehat{\phi_S}\approx\frac{1}{M_S},\widehat{\phi_T}\approx\frac{1}{M_T},\widehat{\phi_\mu}\approx\frac{\sqrt{2}}{M_T}\ [\text{rad}]. \tag{12}$$

Fig. 8 shows that, over the interval $M_T\in[1.01,4]$, $\left|\frac{\phi_\mu-\widehat{\phi_\mu}}{(\phi_\mu+\widehat{\phi_\mu})/2}\right|\times 100\%\le 10\%$ and $\left|\frac{\phi_T-\widehat{\phi_T}}{(\phi_T+\widehat{\phi_T})/2}\right|\times 100\%\le 5\%$. So, the first order approximations are adequate.

Note that, the usual way of expressing percentage relative errors, $\left|\frac{y-\widehat{y}}{y}\right|\times 100\%$, results in infinity when the true value y is 0. Hence the alternative expression above to report errors.

In summary, (3) requires a PM that is $\sqrt{2}$ times that required by (2). That is, $\phi_\mu=\sqrt{2}\phi_\cup$, where $\phi_\cup$ is the PM of ST-union for $M_S=M_T$. For example, for $M_S=M_T=1.1$, $\phi_\cup\approx\frac{1}{M_T}\approx 0.9$ rad$\approx 52°$, while $\phi_\mu\approx 74°$!

2) GM way: Figure 4 shows that S-disc requires a GM $\gamma_S=\frac{M_S}{M_S-1}=\frac{M_T}{M_T-1}$ since $M_S=M_T$, while μ-disc requires a GM $\gamma_\mu=\frac{M_T^2-1}{M_T^2-\sqrt{2M_T^2-1}}$. Denoting the GM of ST-union by $\gamma_\cup$, Fig. 9 shows the ratio $\frac{\gamma_\cup}{\gamma_\mu}$ vs. M_T for $M_T\in[1.01,4]$. Note that $\gamma_\cup=\gamma_S$ for $M_S=M_T$.

Fig. 9 shows that $1<\frac{\gamma_\mu}{\gamma_\cup}\lessapprox 1.1$. Section III-A.1 and Fig. 4 justify the lower limit. In summary, For $M_S=M_T$, μ-disc does not require significantly more GM than does ST-union.

3) Areas: Section III-B.1 shows that, for $M_S=M_T$, $\cos\phi_S=\cos\phi_T$. Therefore, $|\text{AO}|=|\text{CO}|=1$ in Fig. 6, and $d_1=|C_T|-\cos\phi_T=\frac{3M_T^2-1}{2M_T^2(M_T^2-1)}$ and $d_2=1-\cos\phi_T=\frac{1}{2M_T^2}$. Point B is to the right of $(-1,0)$, since $d_2>0$.

Using (9) and $M_S=M_T$ gives $A_\mu=\pi R_\mu^2=\pi\frac{2M_T^2-1}{(M_T^2-1)^2}$. From Fig. 6, $A_\cup=A_{S\,\min}+A_{T\text{maj}}$. Here, $A_{S\,\min}=\frac{R_S^2}{2}(2\theta_S-\sin 2\theta_S)$ is the area of the minor segment (ABCEA) of S-disc, and $A_{T\text{maj}}=\frac{R_T^2}{2}(2(\pi-\theta_T)+\sin 2\theta_T)$ is the area of the major segment (ABCDA) of T-disc, with $\cos\theta_S=\frac{d_2}{R_S}=\frac{1}{2M_T}$, and $\cos\theta_T=\frac{d_1}{R_T}=\frac{3M_T^2-1}{2M_T^3}$. It can be verified that $A_\cup=\frac{1}{M_T^2}\arccos\frac{1}{2M_T}+\frac{M_T^2}{(M_T^2-1)^2}(\pi-\arccos\frac{3M_T^2-1}{2M_T^3})+\frac{\sqrt{4M_T^2-1}}{2M_T^2(M_T^2-1)}$. Fig. 10 shows a plot of $\frac{A_\mu}{A_\cup}$ vs. M_T for $M_T\in[1.01,4]$. This plot shows that $1<\frac{A_\mu}{A_\cup}\le\sqrt{2}$ for $1<M_T\lessapprox\sqrt{2}$, and $\sqrt{2}\lessapprox\frac{A_\mu}{A_\cup}<2$ for $M_T\gtrapprox\sqrt{2}$.

In conclusion, though (2) allows $|w_PS|=|w_TT|$ to be $\sqrt{2}$ times the values allowed by (3) in the worst case, the ratios $\frac{\gamma_\mu}{\gamma_\cup}$ and $\frac{A_\mu}{A_\cup}$ are in general not $\sqrt{2}$; only $\frac{\phi_\mu}{\phi_\cup}$ is.

The next subsection compares (2) and (3) on semilog grid.

C. Characterization on Semilog Grid

This subsection translates the simplified constraints mentioned at the end of Section II-B.3 into open-loop constraints.

1) LF and HF Constraints: Note that $|S|<|F_S|$ is the same as $\frac{1}{|F_S|}<|1+L|$, which implies $\frac{1}{|F_S|}<1+|L|$, or, equivalently, $|L|>\frac{1}{|F_S|}-1$, giving the LF constraint

$$|L|\gtrapprox 1/|F_S|,\ \text{for}\ |F_S(j\omega)|\lessapprox 0.1, \tag{13}$$

Also, $|T|<|F_T| \Leftrightarrow \frac{1}{|F_T|}<|1+\frac{1}{L}| \Rightarrow \frac{1}{|F_T|}<1+|\frac{1}{L}| \Rightarrow |L|<\frac{|F_T|}{1-|F_T|}$ for $|F_T|<1$, giving the HF constraint

$$|L|\lessapprox|F_T|,\ \text{for}\ |F_T(j\omega)|\lessapprox 0.1, \tag{14}$$

These constraints are the LF and HF parts of Fig. 3(a).

The remainder of this paper builds on the loopshaping method for SISO plants that chapters 8 and 12 of [6], [7] present, named here *Besekerskiy-Popov loopshaping* (BPLS). Here is a brief summary of this method.

2) Essence of BPLS in MF Area: For a minimum-phase $G(s)$, and for a specified $M_p\%$, the designer chooses the corresponding M_T from a table, such as Fig. III-B. For this M_T, from the graph of θ vs. $\log_{10}|L|$ of Fig. 11 (b), the designer constructs the phase forbidden region (PFR) and the crossover section of ABMP, as shown in Fig. 12, in the interval $[\omega_{2T},\omega_{3T}]$, and as explained next.

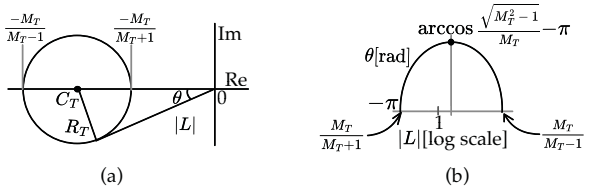


Fig. 11. (a) M_T circle, and (b) the corresponding forbidden region for phase as a function of $|L|$, constructed using figures 5 (a) and (b). The peak value of θ comes from (11) on substituting $\rho{=}\frac{M_T}{M_T^2-1}$ and $r_0{=}\frac{M_T^2}{M_T^2-1}$.

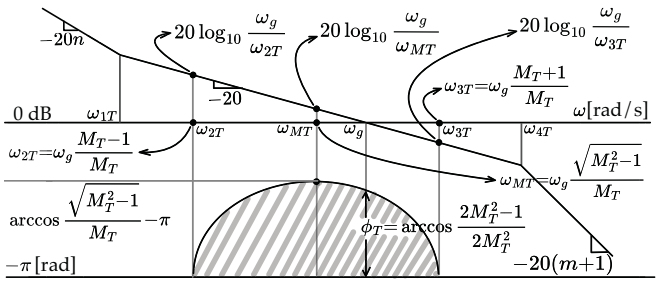


Fig. 12. Constraints from Fig. 11(b) transferred onto the semilog grid.

Choose ω_g such that it helps meet the specified settling time or closed-loop bandwidth or other closed-loop constraints. Through ω_g, draw a straight line of slope -20 dB/dec. This seemingly trivial construction helps associate frequencies ω_{2T}, ω_{MT}, and ω_{3T} with the data from Fig. 11, and thus populate the picture in the interval $[\omega_{2T}, \omega_{3T}]$.

The width of this crossover section is $\log_{10}\frac{\omega_{4T}}{\omega_{1T}}$ decades. This width depends on the neighboring slopes $-20n$ dB/dec (decided by LF forbidden region) and $-20(m{+}1)$ dB/dec (decided by HF forbidden region), and on the peak value of the PFR. Indeed, the minimum-phase TF and phase corresponding to the ABMP of Fig. 12 are

$$\overline{L}(s) = \frac{K(\frac{s}{\omega_{1T}}+1)^{n-1}}{s^n(\frac{s}{\omega_{4T}}+1)^m},$$

$$\angle\overline{L}(j\omega) = -\frac{n\pi}{2} + (n-1)\arctan\frac{\omega}{\omega_{1T}} - m\arctan\frac{\omega}{\omega_{4T}}.$$

This phase has a peak at $\omega{=}\omega^*{=}\sqrt{\frac{(n-1)\omega_{4T}-m\omega_{1T}}{m\omega_{4T}-(n-1)\omega_{1T}}\omega_{1T}\omega_{4T}}$. Frequencies ω_{1T} and ω_{4T} need to be such that $\angle\overline{L}(j\omega^*) \geq \theta^* = \arccos\frac{\sqrt{M_T^2-1}}{M_T} - \pi$. Here, θ^* is the peak of the PFR.

For example, for $n{=}2, m{=}1$, which corresponds to a $\{-40,-20,-40\}$ ABMP, choosing equality sign in the above inequality relates ω_{1T} and ω_{4T} as $\frac{\omega_{4T}+\omega_{1T}}{\omega_{4T}-\omega_{1T}}{=}M_T$ or $\frac{\omega_{4T}}{\omega_{1T}}{=}\frac{M_T+1}{M_T-1}$. The only solution is $\omega_{1T}{=}\omega_{2T}$ and $\omega_{4T}{=}\omega_{3T}$.

BPLS uses such stock loop shapes as in Fig. 12 to meet MF specifications. Joining this particular loop shape to ABMP segments, drawn to satisfy the LF and HF constraints of (13) and (14), results in the complete required $L(s)$. BPLS omits the phase plot, tacitly assuming that $\angle\overline{L}(j\omega)$ stays outside the PFR, provided ω_{1T} and ω_{4T} are such that $\angle\overline{L}(j\omega^*) = \theta^*$.

Remark 3: This assumption is true for $n{=}2, m{=}1$, and needs proving in the general case.

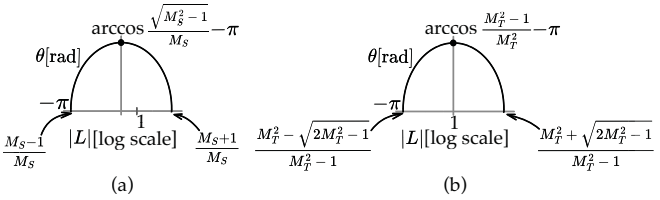


Fig. 13. Forbidden regions analogous to that in Fig. 11(b) with $M_S{=}M_T{>}1$: (a) for S-disc, and (b) for μ-disc.

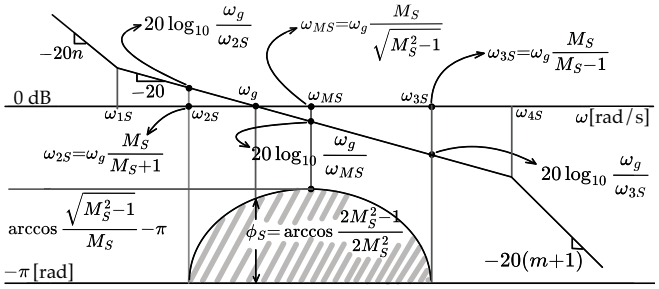


Fig. 14. Constraints from Fig. 13(a) transferred onto the semilog grid, and the corresponding MF loop shape.

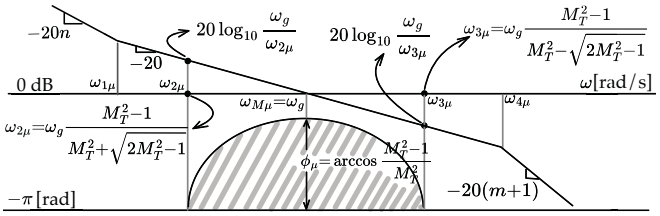


Fig. 15. Constraints from Fig. 13(b) transferred onto the semilog grid, and the corresponding MF loop shape.

The following adapts BPLS to S-disc and μ-disc.

3) MF Loop Shape, given S-disc and μ-disc: Fig. 13 shows the analogs of Fig. 11(b), obtained from S-disc and μ-disc. The procedure of Section III-C.2, used with Fig. 13(a), leads to Fig. 14, and used with Fig. 13(b) leads to Fig. 15. The PFRs in figures 12 and 14 combine to form the PFR due to ST-union, shown in Fig. 16.

Section III-B shows how MSS is conservative relative to CLS. Fig. 16 compares the PFR due to μ-disc with the PFR due to ST-union to further illuminate this conservativeness. Fig. 16 shows that MSS demands more PM than CLS does. ABMP A and ABMP B are of $\overline{L}(s)$ of MSS and CLS, respectively. The available bandwidth Ω_a and the plant's unstable poles upper bound the achievable PM; see figures 7–9 and the related discussion in [8]. In such cases, ABMP B, and not ABMP A, can be the solution. ABMP B represents a nonconservative approach to CLS, and is the second contribution. ABMPs A and B are, respectively, of the TFs

$$\overline{L}_A(s){=}\frac{\omega_g\omega_{2\mu}(\frac{s}{\omega_{2\mu}}+1)}{s^2(\frac{s}{\omega_{3\mu}}+1)},$$

$$\overline{L}_B(s){=}\frac{\alpha\omega_g\omega_{2T}(\frac{s}{\omega_{2T}}+1)(\frac{s}{\alpha\omega_g}+1)}{s^2(\frac{s}{\omega_g/\alpha}+1)(\frac{s}{\omega_{3S}}+1)},\ \alpha{\in}\left(1,\frac{\omega_g}{\omega_{2T}}\right).$$

The next section illustrates this second contribution.

IV. Example

Given that $G(s)$ has $\Omega_a \approx 100$ rad/s, design $L(s)$ for the control system of Fig. 1 to have a bandwidth $\omega_B \geq 0.5$ rad/s, and so that its step response has a steady-state error $e_{\rm ss} \leq 1\%$ and $M_p < 40\%$. Here is a solution direction. Convert these specifications into $F_S(s)$ and $F_T(s)$ of (4) and (5): $A_S = 0.01$ from $e_{\rm ss}$, $M_T = 1.5$ from M_p and Fig. III-B, $\omega_B^* = 0.5$ rad/s from ω_B, and $\omega_{BT}^* = 2$ rad/s from Ω_a. Let $n_1 = 2$, $A_T = 0.01$ and $M_S = M_T$, though they are not specified.

Next, convert $F_S(s)$ and $F_T(s)$ into LF and HF forbidden regions on the loop gain using (13) and (14), and PFRs, with $\omega_g = \sqrt{\omega_B^* \omega_{BT}^*} = 1$ rad/s, as in Fig. 16. Note that MSS demands $\sqrt{2}$ times more PM than needed by the CLS problem. The final solutions are $L_\mu(s) = \overline{L}_A(s)$ (MSS) and $L_\cup(s) = \overline{L}_B(s)$ (CLS), with $\alpha = 1.17$, and give the results in Fig. 17. The plot of $\angle L_\cup(j\omega)$ is tangential to the PFR due to ST-union. The m_S and m_T corresponding to $L_\cup(s)$ are closer to M_S and M_T, than are the m_S and m_T corresponding to $L_\mu(s)$. For $1.1 \leq M_T \leq 1.5$, the settling time using $L_\cup(s)$ is about $\frac{1}{\sqrt{2}}$ times that using $L_\mu(s)$.

V. Conclusion

The improvement that this paper has demonstrated (PM not much more than needed, and reduced settling time) over MSS is thanks to using a higher order controller judiciously. The PFR due to μ-disc does not allow MSS to deliver this improvement even using a higher-order controller.

The remarks in the paper show ways to make this work complete. Here are additional directions for future research. This paper has considered a $\{-20n, -20, -20(m+1)\}$ MF ABMP, with $n = 2, m = 1$ for illustration. Future work can generalize this methodology to higher values of n and m. The paper has determined PFRs corresponding only to the lower halves of S-disc, T-disc, and μ-disc. Future work can address the upper halves too. In that exercise, in addition to PM, GM, and disc dimensions, the number of encirclements of the critical point may matter [13].

Appendix

A. Proof of $|m_S - m_T| \leq 1$

Equation (1) gives $S(j\omega) + T(j\omega) = 1$, $\forall \omega$. Hence, $||S(j\omega)| - |T(j\omega)|| \leq S(j\omega) + T(j\omega) = 1$, $\forall \omega$. The value of m_S is such that $\max_\omega |S(j\omega)| \leq m_S$. If $m_S \geq m_T$, then $m_S - |T(j\omega)| \leq 1$, $\forall \omega$. Since this inequality is valid for all ω, it is also valid for the case of $|T(j\omega)|$ being maximum. Hence, $m_S - m_T \leq 1$, as $\max_\omega |T(j\omega)| \leq m_T$. Similarly, $m_T - m_S \leq 1$ when $m_T > m_S$. In summary, irrespective of whether $m_S < m_T$ or $m_S > m_T$, $|m_S - m_T| \leq 1$.

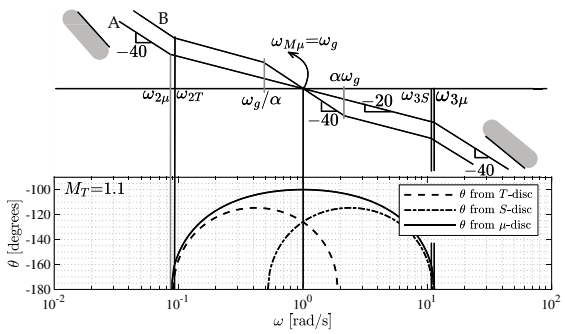


Fig. 16. MF loop shape and PFRs of the ST-union and the μ-disc. Section III-C.1 gives the LF and HF magnitude forbidden regions.

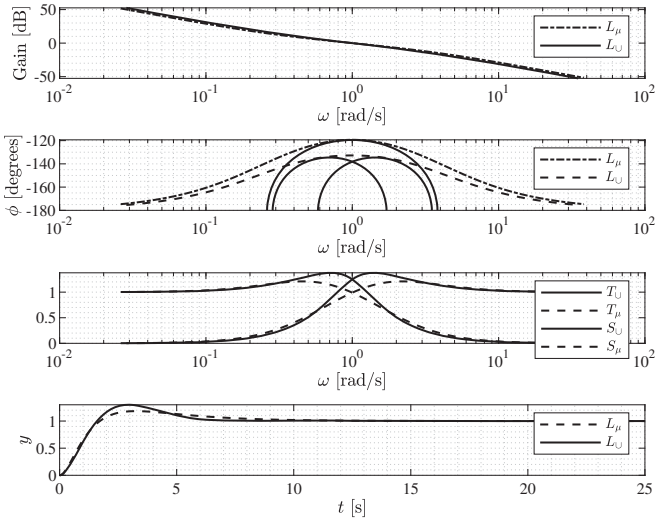


Fig. 17. Loop gain, loop phase, sensitivity and complementary sensitivity functions, and closed-loop step response in the example.

References

[1] Boris J Lurie and Paul Enright. *Classical Feedback Control with Nonlinear Multi-Loop Systems: With MATLAB and Simulink*. CRC Press, 3rd edition, 2019.

[2] Sigurd Skogestad and Ian Postlethwaite. *Multivariable Feedback Control: Analysis and Design*. Wiley, 2nd edition, 2005.

[3] John C Doyle, Bruce A Francis, and Allen R Tannenbaum. *Feedback Control Theory*. Courier Corporation, 2013.

[4] Gene Franklin, J. David Powell, and Abbas Emami-Naeini. *Feedback Control of Dynamic Systems*. Pearson Education, 5th edition, 2008.

[5] Katsuhiko Ogata. *Modern Control Engineering*. Pearson Education, 4th edition, 2002.

[6] V.A Besekerskiy and E.P. Popov. *Teoriya Sistem Avtomaticheskogo Regulirovaniya*. Nauka, Moscow, 3rd edition, 1975. In Russian.

[7] V.A Besekerskiy and E.P. Popov. *Teoriya Sistem Avtomaticheskogo Upravleniya*. Professiya, Saint Petersburg, 4th edition, 2003. http://publ.lib.ru/ARCHIVES/B/BESEKERSKY_Viktor_Antonovich/_Besekerskiy_V.A..html. In Russian.

[8] Gunter Stein. Respect the Unstable. *IEEE Control Systems Magazine*, 23(4):12–25, 2003.

[9] Jong Nam Yun and Jian-Bo Su. Design of a disturbance observer for a two-link manipulator with flexible joints. *IEEE Transactions on Control Systems Technology*, 22(2):809–815, 2013.

[10] Jeffrey T Csank and Thomas J Stueber. Shock position control for mode transition in a turbine based combined cycle engine inlet model. Technical Report NASA/TM-2013-217824, NASA, 2013.

[11] Simone Vidano *et al*. Drag-Free and Attitude Control System for the LISA Space Mission: An H_∞ Constrained Decoupling Approach. *IEEE Transactions on Control Systems Technology*, 2024.

[12] Mathworks. Mixed-Sensitivity Loop Shaping, Matlab R2024a. https://in.mathworks.com/help/robust/gs/using-mixsyn-for-h-infinity-loop-shaping.html, 2024.

[13] Girish Deodhare and Vijay Patel. A "modern" look at gain and phase margins: An H_∞/μ approach. In *Guidance, Navigation, and Control Conference and Exhibit*, pages 325 – 335, Boston, 1998. AIAA.

[14] Vincent Besson and Andrew Thomas Shenton. An interactive parameter space method for robust performance in mixed sensitivity problems. *IEEE Transactions on Automatic Control*, 44(6):1272–1276, 1999.

[15] William Messner. Some advances in loop shaping controller design with applications to disk drives. *IEEE Transactions on Magnetics*, 37(2):651–656, 2001.